

## THE BEHAVIOR OF THE CFS-ZEE SECTION UNDER MONOTONIC AXIAL LOAD: AN EXPERIMENTAL AND PARAMETRIC STUDY

Anwar Badawy Badawy Abu-Sena<sup>1</sup>, Hanan Hussien El-Tobgy<sup>1\*</sup>, Emad Darwish<sup>1</sup>, Andrew Nabil<sup>1</sup>

<sup>1</sup> Civil Engineering Department Faculty of Engineering at Shoubra Benha University, Cairo, Egypt.

\*Corresponding author's E-mail: nsae1986@hotmail.com

Received :16 March 2022 Accepted:17 April 2022

### ABSTRACT

Currently, the cold-formed Steel sections (CFS) are increasingly used in light and mid-height buildings. So, this research examined the axial compression behavior of CFS thin-walled Zee-shaped section under pure axial monotonic loading. This study conducted full-scale tests on three specimens to investigate the three main modes of failure: local buckling, distortion buckling, and global buckling modes. The specimens were selected from CFS Zee sections with 600mm, 1000mm, and 2500mm. The imperfection of the CFS sections was captured by the 3D scanning before testing and implementation in the FE models. Then, the pure axial load was applied monotonic. The failure modes and axial capacity are discussed in detail. In addition, this research investigated the axial load-displacement responses and the axial load capacity. The energy dissipation with strength degradation was thoroughly investigated. A Finite Element Model (FEM) was conducted and verified by the experimental results. Finally, the FEM analysis was extended to study the behavior of the Zee section with a different range of dimensions to predict the section parameters' behavior under axial monotonic load.

**KEYWORDS:** Cold-formed Steel, Zee Section, monotonic loading, 3D scanning, global buckling, distortion buckling, local buckling.

السلوك المحوري لعناصر مقاطعات الصلب البارد "Zee" تحت تأثير حمل مركزي: اختبارات معملية وبراميتريه

انور بدوي بدوي ابو سنه<sup>١\*</sup>، حنان حسين التوبجي<sup>٢</sup>، عماد درويش<sup>٣</sup>، اندرو نبيل<sup>٤</sup>

قسم الهندسة المدنية، كلية الهندسة بشبرا، جامعة بنها، القاهرة، مصر.

\* البريد الإلكتروني للمؤلف الرئيسي: nsae1986@hotmail.com

### الملخص

هذه الايام، يتم استخدام المقاطع الفولاذية المشكلة على البارد (CFS) بشكل متزايد في المباني الخفيفة والمتوسطة الارتفاع. ولذلك، فحص هذا البحث السلوك للضغط المحوري لقسم Zee ذي السمكات الرقيقة (CFS) تحت تحميل أحادي محوري. أجرت هذه الدراسة اختبارات واسعة النطاق على ثلاث عينات للتحقق من الأنماط الرئيسية الثلاثة للفشل: الانثناء المحلي، والتواء التشوه، وأنماط الانثناء الشاملة. تم اختيار عينات CFS Zee بطول ٦٠٠ مم و ١٠٠٠ مم و ٢٥٠٠ مم. تم التقاط التشوهات في المقاطعات من خلال المسح الضوئي

ثالثي الأبعاد قبل اختبارها وتنفيذها في نماذج FE. بعد ذلك، تم تطبيق الحمل المحوري المركزي بشكل منتظم. تمت ملاحظة أوضاع الفشل والمقاومة القطاع المحورية. بالإضافة إلى ذلك، فحص هذا البحث الاستجابات المحورية للحمل والإزاحة وقدرة التحميل المحورية. تم التحقق بدقة في تبديد الطاقة مع تدهور القوة. تم إجراء نموذج عنصر محدود FEM والتحقق من النتائج التجريبية. أخيرًا، تم تمديد تحليل FEM لدراسة سلوك القطاعات الصلب على البارد بمجموعة مختلفة من الأبعاد للتنبؤ بالتصرف القطاعات تحت الحمل الرأسي المحوري.

**الكلمات المفتاحية:** الصلب المشكل على البارد ، تحميل راسي ، مسح ثلاثي الأبعاد ، انحناء عالمي ، انحناء تشويه ، انحناء محلي.

## 1. Introduction

Cold-formed steel (CFS) thin-walled sections have been increasingly popular in recent years. They are widely employed in current building systems due to their lightweight and high strength advantages with less effort to create varied section shapes. CFS sections are provided to support vertical and horizontal loads in low-rise buildings as they provide easy installation and recyclability [1-3]. In addition, the behavior of the individual components of thin-walled sections can be used to examine these sub-elements. Compressive loads cause inelastic buckling deformation in CFS members, reducing their strength and stiffness [4-7]. ABAQUS's nonlinear finite element modeling explores the effects of slenderness, imperfection, and loaded boundary conditions on cyclic response and energy dissipation [8, 9]. The Zee section, on the other hand, is rarely studied; most past research has focused on lipped channel and box sections.

## 2. Experimental Programs

### 2.1. Specimen Preparation

A Zee section (200Z20) is evaluated in the experimental program in this study. The 200Z20 has a total web depth of 200 mm, a 60 mm flange width, a 20 mm lip length at 45 degrees, and a 2 mm nominal sheet thickness, as shown in **Fig. 1**. Because the Zee section is primarily controlled by local buckling on the web, a notch is added to the web, as shown in **Fig. 1 (b)**, to prevent the performance of local buckling at the web before the formation of distortion or global buckling. The length (L) of the specimen is used to isolate each buckling limit state. According to the American Iron and Steel Institute (AISI) [11], and by using the direct strength method DSM, the predicted compression capacity of the CFS Zee-sections is governed by the local, distortional, or global buckling. The mechanical properties of the 200Z20 section are summarized in **Table 1** for the Zee Section with or without a notch.

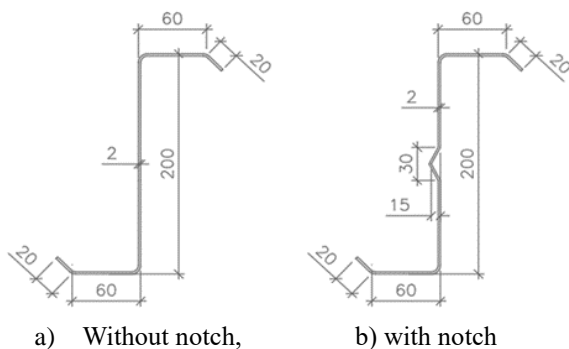
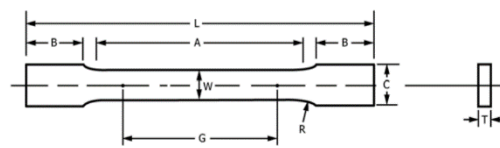


**Fig 1. Zee section with or without notch**



Where, G—Gauge length  $50.0 \pm 0.1$  mm  
W—Width  $12.5 \pm 0.2$  mm, T—Thickness of material  
R—Radius of fillet, 12.5 mm, L—Overall length, 200 mm,  
A—Length of the reduced parallel section, 57 mm  
B—Length of grip section, 50 mm  
C—Width of grip section, 20 mm

**Fig 2. Tensile Testing Machine**

**Table 1 Cold-formed Zee Section Properties**

Section	Area mm <sup>2</sup>	Weight KN/m	I <sub>x</sub> mm <sup>4</sup>	I <sub>y</sub> mm <sup>4</sup>	I <sub>xy</sub> mm <sup>4</sup>	C <sub>w</sub> mm <sup>6</sup>	J mm <sup>4</sup>
<b>200Z2</b>	692.46	0.05348	4123508	601495	1144825	4.19E+09	927.3
<b>200Z2 with Notch</b>			4039221	602535	1134372	4.13E+09	931.6

## 2.2. Material Properties and Specimen Dimensions

CFS specimens are divided into three sets: one for local buckling, the second for distortion buckling, and the third for global buckling that is subjected to monotonic displacement (pure axial compression). Specimen with 600mm long without a notch on the web is failed due to local buckling. Specimen with 1000mm long and a notch in the web is failed due to distortion buckling. Specimen with 2500mm long and a notch in the web failed due to global buckling. Then, a finite strip Eigen-buckling analysis software, CUFSM [12], uses section dimension and length to calculate the elastic buckling loads for local buckling,  $P_{cr}$ , distortional buckling,  $P_{crd}$ , and global buckling,  $P_{cre}$ , and the associated half-wavelengths ( $L_{cr}$ ,  $L_{crd}$ , and  $L_{cre}$ , respectively) that are summarized in **Table 2**.

**Table 2 Zee Buckling Properties Regarding  $F_y = 420\text{MPa}$**

Buckling Mode	200Z2				200Z2 With Notch			
	Magnitude	Stress	Stress	Length	Magnitude	Stress	Stress	Length
	(kN, kN-m)	(MPa)	/ Yield	(mm)	(kN, kN-m)	(MPa)	/ Yield	(mm)
$P_{crl}$	76.37	109.5	0.2607	152.14	384.63	534.7	1.2731	73.11
$P_{crd}$	101.32	145.3	0.3459	434.45	138.62	192.7	0.4588	621.56
$M_{crlx+}$	11.98	289.2	0.6887	109.43	19.14	461.9	1.0997	70.8
$M_{crdx+}$	174	---	-----	-----	174.05	---	-----	----
$M_{crlx-}$	11.98	289.2	0.6887	109.43	18.57	448.1	1.0669	69.54
$M_{crdx-}$	174	---	-----	-----	174.05	---	-----	----
$M_{crly+}$	6.43	781.2	1.8599	108.33	9.94	1210	2.881	68.14
$M_{crdy+}$	3.65	443.5	1.056	446.67	3.89	473.9	1.1284	428.97
$M_{crly-}$	6.43	781.2	1.8599	108.33	10.56	1286	3.0622	49.15
$M_{crdy-}$	3.65	443.5	1.056	446.67	3.98	485.2	1.1552	443.54

$P_{crl}$  = Critical Axial Local buckling load,  $P_{crd}$  = Critical Axial Distortion buckling load

$M_{crlx+}$  /  $M_{crlx-}$  = Critical Flexure Local buckling load top and bottom about the major axis

$M_{crdx+}$  /  $M_{crdx-}$  = Critical Flexure distortion buckling load top and bottom about the major axis

$M_{crly+}$  /  $M_{crly-}$  = Critical Flexure Local buckling load top and bottom about the minor axis

$M_{crdy+}$  /  $M_{crdy-}$  = Critical Flexure distortion buckling load top and bottom about the minor axis

The steel employed in the studies was evaluated experimentally by performing coupon tests on five randomly selected samples. A GALBADINI test machine with a maximum tension capacity of 10 tones was employed to apply the load during the tests. The coupon tests followed instructions according to

ASTM E8M-16. Flat portions of the web and flanges were first rough cut with a metal band saw, as shown in **Fig. 2**, and then finished the dimensions with CNC milling machines. Tensile coupons were positioned in the machine with friction grips. They were ensured that each specimen was aligned vertically and horizontally between the grips. The data was converted to tensile force and engineering strain using the conversion factors. Then data was plotted on the screen and recorded in the file. The average tensile yield stress was determined from the coupon test for the CFS zee section.

### 2.3. Specimens' imperfection

As the initial deformation of the structure plays a significant role during the structural analysis, a complete three-dimension scanning was considered for the cold-formed zee section to measure all relevant imperfections with high effectiveness and accuracy. First, the specimens are set up for testing. Then, individual scans are taken around the specimens, registering the individual scan of local points to complete the 3D models of points with a global coordinate system. Finally, the computer programmers were captured to make sense of the 3D points clouds. Each point represented a single laser scan location measurement collected together, creating a complete scene captured using the registration process.

Point clouds are a means of collating many single spatial measurements into a dataset that can then represent a whole. Their cloud points represent the three coordinates (x, y, and z) of a single point on an underlying sample surface; when color information was considered, the point cloud became four-Dimension scanning. Light detection and ranging (LiDAR) technology was used to generate points clouds. **Fig. 3** illustrates the relevant geometric imperfections with point clouds. After registration and collecting data, information is of point clouds; it is cleaning off all noising points and elements that do not belong to specimens. **Fig. 4** presents the measurement of imperfection using the "Recap" program. In the Finite element models, imperfections ought to be included. Additionally, it should account for the outcomes of geometric deviations from the ideal form of the structure for CFS and boundary condition defects if determined.

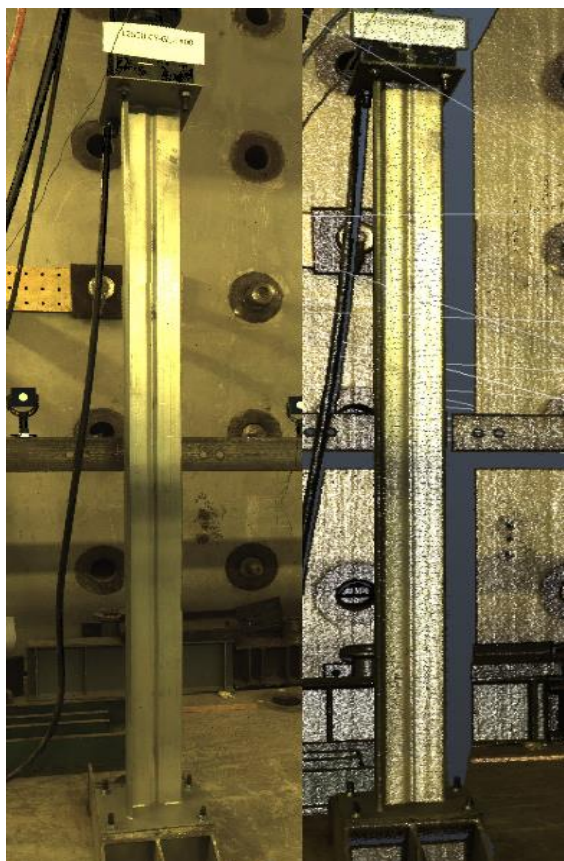


Fig 3. Difference between actual capture and point Cloud for L2500CYDSEX00



Fig 4. Using Recap Point Cloud programs to measure imperfection of specimens

The cross-section dimensions were assigned in the finite strip Eigen-buckling analysis software (CUFSM). Specimen nomenclature is illustrated in Fig. 5. The element boundary conditions were considered fixed-fixed when calculating the elastic buckling loads. Therefore, an effective buckling length of  $0.5L$  is considered when calculating  $P_{cre}$ . The average values of imperfection measured that are summarized in Table 3.

Table 3 Summary of Measured Cross-Section Dimensions

Specimen	S1	S2	S3	S4	S5	L1	L2	L3A	L3B	L3C	L4
	Degree (°)					mm					
L600MNLCEX00	129	89	94	132	--	16	53	187	55		16
L1000MNDSEX00	138	94	91	131	180	18	54	78	32	69	52
L2500MNGLEX00	135	93	91	135	180	16	58	76	29	78	55



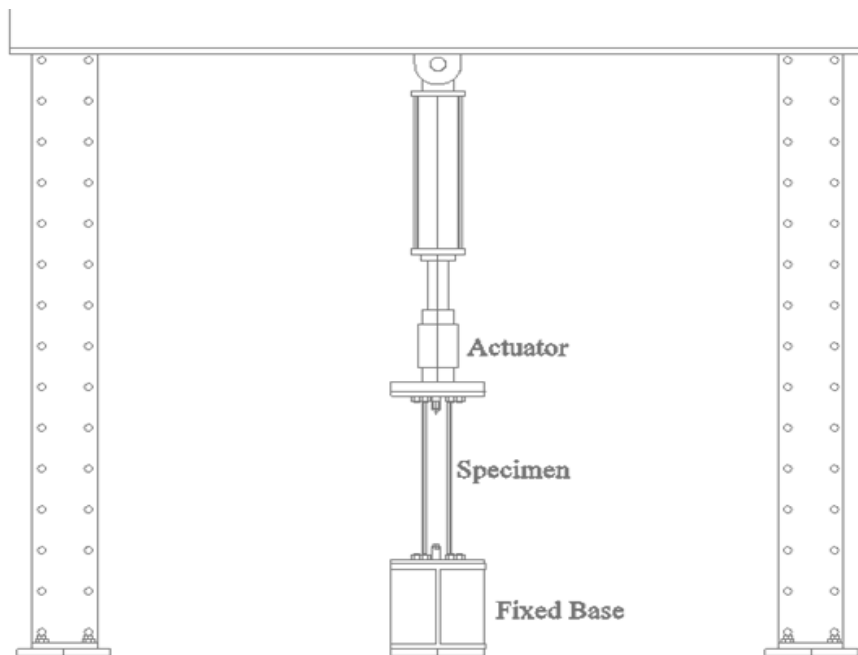


Fig 6. Specimen Setup

## 2.5. Specimens' selection

The local buckling was predicted by DSM considering the initial slenderness of local buckling is  $\lambda_l = 0.776$ , and the distortional buckling deformation initiates at  $\lambda_d = 0.561$ . Using  $\lambda = (P_e/P_{cr})^{0.5}$ , then  $P_e = 0.60P_{cr1}$  and  $P_e = 0.31P_{crd}$ . The global buckling deformation influences load-deformation response at  $P_e = 0.50P_{cre}$ . CUFSM is used to calculate the controlled buckling mode of specimens subjected to pure axial with different lengths, with and without notches, as shown in Fig.7.

CFS-200Z2 with a length 600mm is subjected to web local buckling, while the same section, but with web notch, is subjected to distortion and global buckling. 200Z2 specimens with lengths 1000 and 2500 mm were selected to study the distortion and global buckling. Specimen displacements were measured by five LVDTs connected along the length of the specimens, as shown in Fig. 8 and as summarized in Table 4.

The displacement rate of  $0.0001(\text{mm/mm})/(\text{min})$  is used for the monotonic loading test, which forms a maximum rate of 21MPa per minute, as recommended by the AISI-S910-08 test method. This monotonic rate test produces tensile yield stresses about 2% larger than the static tensile yield stress.

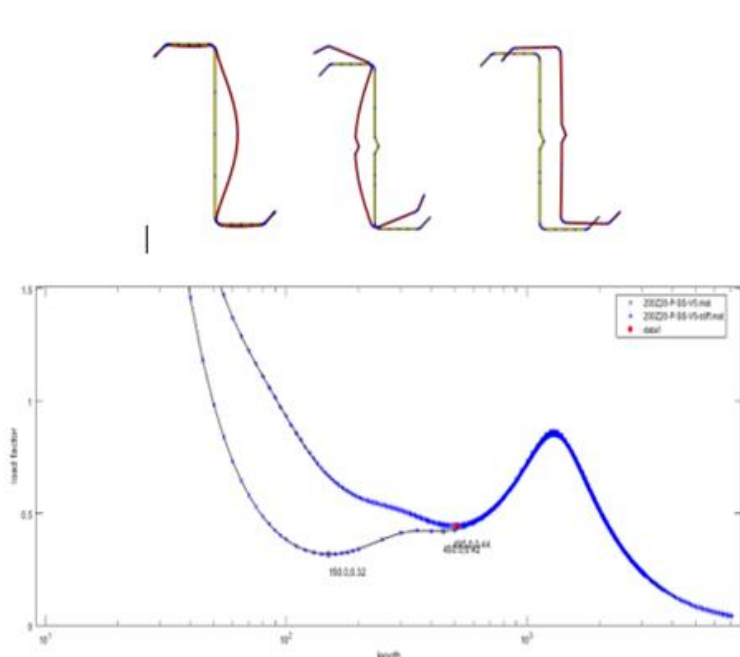


Fig. 7 The elastic buckling curve of 200Z2 subjected to pure axial with or without web stiffeners for lengths 600, 1000, 2500 mm, respectively

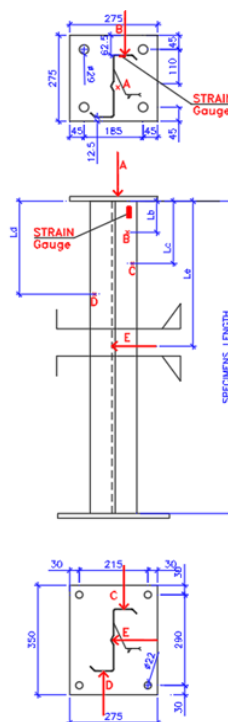


Fig. 8 LVDT and strain gauge locations

Table 4 LVDT location at Specimens

Specimen	Lc	Ld	Lb	Le
	mm	mm	mm	mm
L600MNLCEX00	300	300	150	300
L1000MNDSEX00	200	200	100	500
L2500MNGLEX00	1250	1250	1250	1250

### 3. Experimental Results

The monotonic response of axial load-displacement ( $P-\delta$ ) for each model was evaluated. The responses were characterized to define strength and stiffness deterioration, and hysteretic energy dissipation. The specimens had linear behavior until peak load, associated with strength and stiffness degradation.

In the case of local buckling specimens, not pure local buckling occurs but also contributes to distortion in the flange of the zee section, As the specimen length exceeds the critical length for local buckling  $L_{cr}$ . In the monotonic situation of specimens of 600 mm length, the web local buckling and deformation occurred at the lower part of the specimen, and they tended to flange, as shown in **Fig. 9(a)**. **Fig.9(d)** represents the deformed shape by FEM.

The flange with lip has at least two half-wavelength at mid-length of the specimens with 1000 mm lengths, as shown in **Fig. 9(b)** and **Fig. 9(e)**. Local buckling in the web is prevented by the web notch, while distortion buckling is controlled. Strength and stiffness degraded from inelastic strains presented accumulated damage half-wave. Plastic deformation was formed before the specimens reached their maximum capacity, followed by post-buckling behaviors, and concentrated at corners between web and

THE BEHAVIOR OF THE CFS-ZEE SECTION UNDER MONOTONIC AXIAL LOAD: AN EXPERIMENTAL AND PARAMETRIC STUDY

flanges.

Specimens with 2500mm length performed global flexure torsion buckling of one half-wavelength at the specimens' mid-length. The distorted curvature of the flange and ripping in the lip are both associated with global buckling, as shown in **Fig. 9(c)**, and corresponding FEM are illustrated in **Fig. 9(f)**.

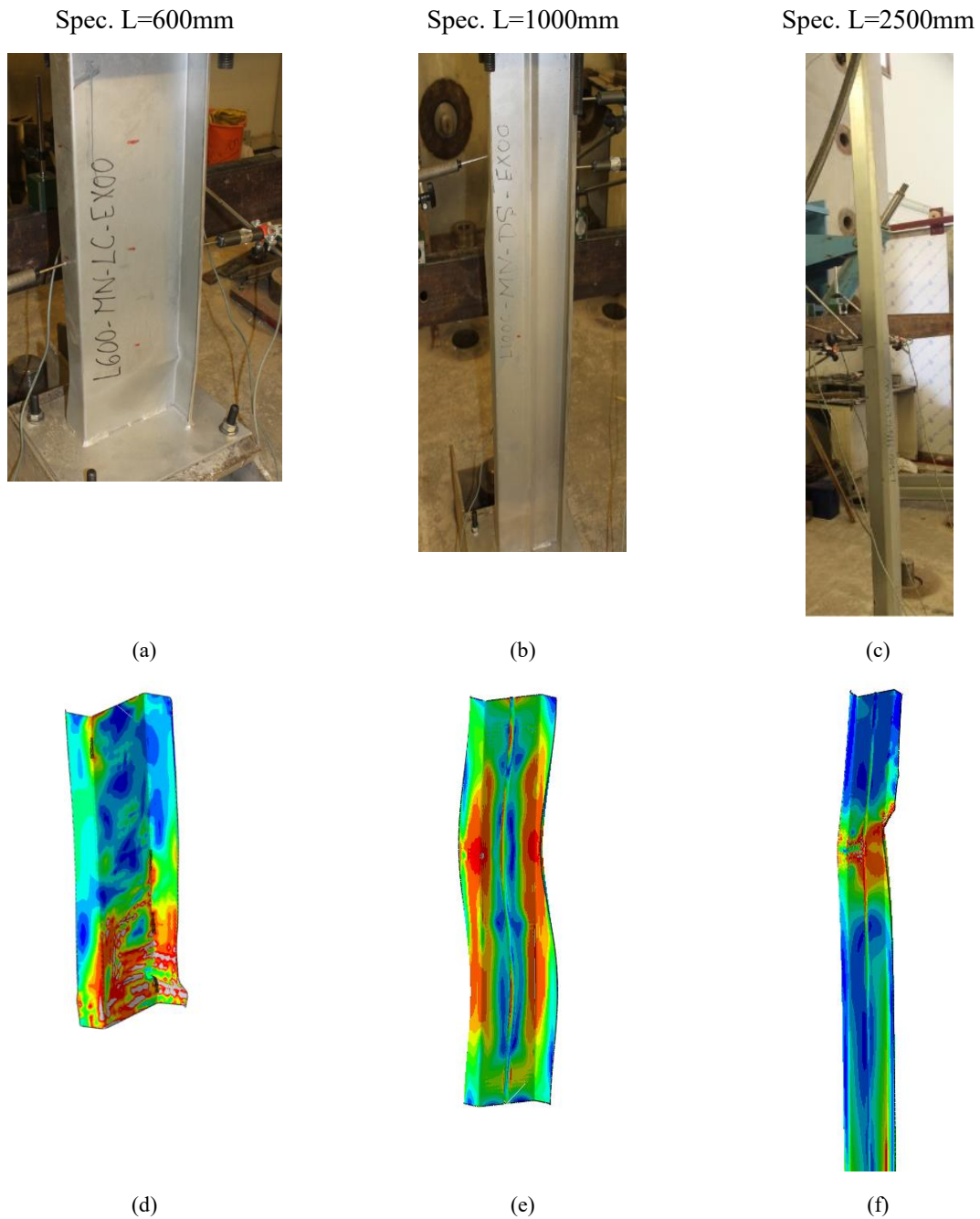


**Fig 9. Verification of buckling mode of Experimental against Finite Element Models (FEM)**

#### 4. Verifications

A Finite Element Model, FEM for the CFS zee section under axial monotonic loading, was performed using the ABAQUS soft package. The FEM outcomes were compared with the experimental results for verification. **Table 5** shows the comparisons for the peak capacity in compression of monotonic loading cases for both experimental and FEM results. The Means and Coefficient of variation COV for  $P_{\text{Max-Test}}/P_{\text{max-FE}}$  was equal to 1.03 and 0.05 for compression. It can be concluded that the FEM can be used to investigate the cold-formed behavior as experimental circumstances were accurately represented.

The analysis is based on plasticity models using Von Mises yield surface, and combined hardening parameters with four back stresses were assigned for material behavior for all specimens. In addition, isotropic and kinematic hardening material models were adopted with an equation expressed by Zub and Stratan [13], adapting the tensile coupon test properties. Finally, the damage and fracture mechanisms were applied to the FEM. The damage and its propagation until fracture or tearing of the material was assigned in ABAQUS using the ductility damage and damage evolution commands. Metal sheet damage initiation was implemented using the Bao-Wierzbicki fracture criteria [14, 15].

**Table 5 Experimental and FE results for cold-formed under cyclic load**

	$P_{\text{max-Test}}$ (KN)	$\delta_{\text{max-Test}}$ (mm)	$P_{\text{max-FE}}$ (KN)	$\delta_{\text{max-FE}}$ (mm)	$P_{\text{max-Test}}/P_{\text{max-FE}}$
L600-MN-LC	128.3	1.27	121	1.24	1.06
L1000-MN-DS	113.6	3.01	117.6	2.22	0.97
L2500-MN-GL	82.9	3	78.2	3.05	1.06
Mean for Specimens					1.03
Standard deviation for Specimens					0.052
COV for Specimens					0.05

$P_{\text{max-test}}, \delta_{\text{max-test}}$ = ultimate capacity in compression and corresponding displacement from experimental  
 $P_{\text{max FE}}, \delta_{\text{max FE}}$ = ultimate capacity in compression and corresponding displacement from the FE model

#### 5. Parametric Study:

A comprehensive parametric study was carried out to thoroughly understand the behavior of the CF-Zee section under monotonic load. It is generated by changing the Flange width (FL) by 60, 80, and 100mm, the Lip depth (LIP) by 10,20, 30, and the thickness (T) by 1,2, 3, and 4mm. The numerical model considered the three buckling modes by adapting elements' lengths L=600, 1000, and 2500mm to investigate the local, distortion, and global buckling modes.

The studied models were considered fixed at both ends. At the loading point, load-displacement curves were extracted for each parameter, as shown in **Fig.10**. In the case of local buckling, the strength and stiffness decrease faster than distortion specimens after reaching the peak capacity. Local and distortion specimens lose about 60% to 70% of their maximum capacity. While, in the case of global buckling, they lose about 40% to 50% of the peak capacity. Increasing the thickness has more advantages in local and distortion specimens than in global specimens.

**Fig. 11**, represents the relation between the peak capacities to the yielding capacity ( $P/P_y$ ) for all specimens with the flange width to depth (b/d) considering the change of thickness effect (thickness T= 1mm and 2mm). It is noticed that the section capacity ( $P/P_y$ ) in local and distortion buckling (L600 and

THE BEHAVIOR OF THE CFS-ZEE SECTION UNDER MONOTONIC AXIAL LOAD: AN EXPERIMENTAL AND PARAMETRIC STUDY

L1000) decreased with the increasing slenderness ratio ( $b/d$ ). In the global buckling models, the section capacity at ratio 0.5 for  $b/d$  to capture maximum advantages. Moreover, increasing the lip length from 10mm to 20mm increases the section capacity by 35%. Increasing lip depth from 20 to 30mm leads to increasing section capacity by about 10%.

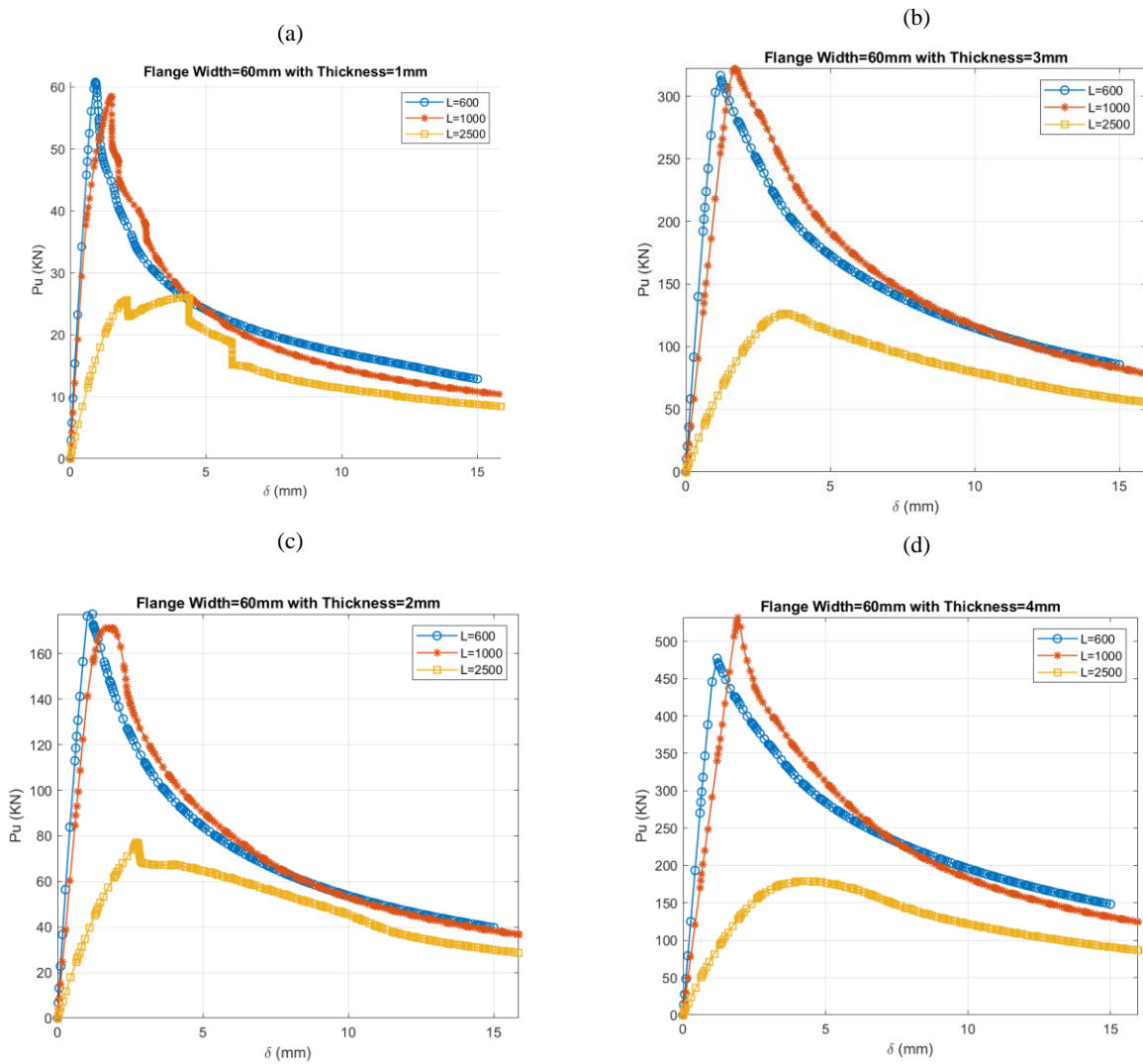


Fig.10 P- $\delta$  relation for each buckling mode for CFS-zee sections with different thicknesses

THE BEHAVIOR OF THE CFS-ZEE SECTION UNDER MONOTONIC AXIAL LOAD: AN EXPERIMENTAL AND PARAMETRIC STUDY

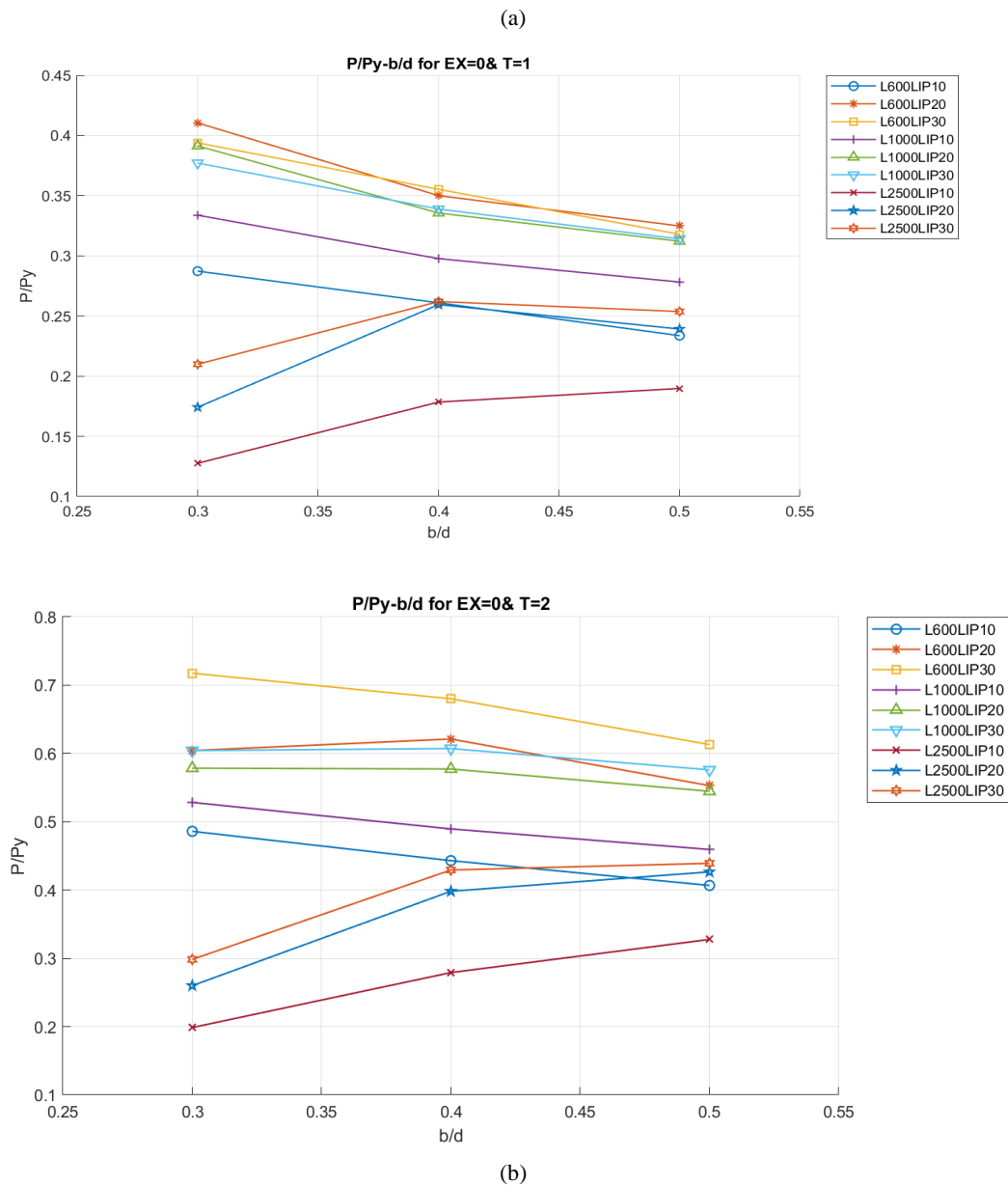


Fig. 11. Ultimate section capacity to yielding capacity ( $P/Py$ )

## 6. Conclusion

This study investigated the response of CFS-Zee elements subjected to axial compression monotonic loading. The Element lengths were chosen with lengths 600, 1000, and 2500mm to identify the local, distortion, and global buckling modes for each specimen, the load-deformation response, strength deterioration, and energy dissipation properties of CFS axial members were evaluated using three monotonic compression tests.

The point clouds were conducted on the 3D FEM to accurately measure all the relevant imperfections. A FEM was performed by Abaqus software and verified by the experimental findings. Finally, a parametric study was conducted for CFS-Zee sections with different thicknesses, flange width, lip depth, and element lengths. Following is a summary of the findings:

THE BEHAVIOR OF THE CFS-ZEE SECTION UNDER MONOTONIC AXIAL LOAD: AN EXPERIMENTAL AND PARAMETRIC STUDY

1. The stress concentration in the bottom of the web of local buckling specimens, and between flanges and web in distortion specimens, and at mid-height in global.
2. The global Specimen associated with distortion behavior.
3. The web local buckling occurred along the specimens associated with flanges' distortion in local buckling specimens.
4. In distortion buckling specimens, it is noticed that there are two waves of distortion for both flanges associated with lip opening, and there is no local buckling occurred due to web notch stiffening.
5. Local and distortion specimens sustained about 30% to 40 % capacity after reaching the peak capacity. In comparison, global buckling specimens sustained about 50% to 60% of the section capacity.
6. From the parametric study results, as the thickness increase, the CFS zee section can sustain more load after peak capacity and become more valuable in distortion specimens' capacity than local buckling specimens.
7. Increasing the slenderness ratio of a flange to depth ( $b/d$ ) decreases the section capacity to yield local and distortion buckling specimens.
8. The optimum ( $b/d$ ) ratio was about 0.5 for the zee section subjected to pure axial for global buckling specimens.

## References

- [1] Zhang, X., E. Zhang, and C. Li. Study on axial compression mechanical behavior of cold-formed thin-walled C-shaped steel composite wall sheathed with straw board on both sides. in *Structures*. 2021. Elsevier.
- [2] Zhang, J.-F., et al., Experimental study on seismic performance of the connection for ATLS modular house. *Journal of Constructional Steel Research*, 2020. 170: p. 106118.
- [3] Iuorio, O., L. Fiorino, and R.J.T.-w.s. Landolfo, Testing CFS structures: The new school BFS in Naples. 2014. 84: p. 275-288.
- [4] Zhang, W., et al. Influencing factors analysis on shear capacity of cold-formed steel light frame shear walls. in *Structures*. 2021. Elsevier.
- [5] Derveni, F., S. Gerasimidis, and K.D. Peterman, Behavior of cold-formed steel shear walls sheathed with high-capacity sheathing. *Engineering Structures*, 2020. 225: p. 111280.
- [6] Shamim, I. and C.A. Rogers, Steel sheathed/CFS framed shear walls under dynamic loading: Numerical modelling and calibration. *Thin-Walled Structures*, 2013. 71: p. 57-71.
- [7] Wang, J., et al., Cyclic test and numerical analytical assessment of cold-formed thin-walled steel shear walls using tube truss. *Thin-Walled Structures*, 2019. 134: p. 442-459.
- [8] Padilla-Llano, D.A., C.D. Moen, and M.R. Eatherton, Cyclic axial response and energy dissipation of cold-formed steel framing members. *Thin-Walled Structures*, 2014. 78: p. 95-107.
- [9] Padilla-Llano, D.A., M.R. Eatherton, and C.D. Moen, Cyclic flexural response and energy dissipation of cold-formed steel framing members. *Thin-Walled Structures*, 2016. 98: p. 518-532.
- [10] Schafer, B.W., The direct strength method of cold-formed steel member design. *Journal of constructional steel research*, 2008. 64(7-8): p. 766-778.
- [11] Institute, A.I.S., AISI-S100-16: North American specification for the design of cold-formed steel structural members. 2016, ANSI/AISI Washington, DC.
- [12] Schafer, B., CUFSM 5.01—Elastic Buckling Analysis of Thin-walled Members by the Finite Strip Method and Constrained Finite Strip Method for General End Boundary Conditions. Department of Civil Engineering, Johns Hopkins University. Department of Civil Engineering,

THE BEHAVIOR OF THE CFS-ZEE SECTION UNDER MONOTONIC AXIAL LOAD: AN EXPERIMENTAL AND  
PARAMETRIC STUDY

2012.

- [13] Zub, C., A. Stratan, and D. Dubina, Calibration of parameters of combined hardening model using tensile tests. 2020.
- [14] Bao, Y., Wierzbicki, Tomasz On fracture locus in the equivalent strain and stress triaxiality space. *International Journal of Mechanical Sciences*, 2004. 46(1): p. 81-98.
- [15] Lee, Y.-W., T.J.M.I.o.T. Wierzbicki, Impact, and C.L. Report, Quick fracture calibration for industrial use. 2004(115).